Applied Catalysis B: Environmental 168-169 (2015) 114–124

Contents lists available at ScienceDirect

Applied Catalysis B: Environmental

journal homepage: www.elsevier.com/locate/apcatb

Role of chlorophyll in *Spirulina* on photocatalytic activity of CO_2 reduction under visible light over modified N-doped TiO_2 photocatalysts

Thanaree Phongamwong[a], Metta Chareonpanich[a,b,c,*], Jumras Limtrakul[b,c]

[a] Department of Chemical Engineering, Faculty of Engineering, Kasetsart University, Bangkok 10900, Thailand
[b] Center for Advanced Studies in Nanotechnology for Chemical, Food and Agricultural Industries, Kasetsart University, Bangkok 10900, Thailand
[c] PTT Group Frontier Research Center, PTT Public Company Limited, Bangkok 10900, Thailand

ARTICLE INFO

Article history:
Received 6 November 2014
Received in revised form 8 December 2014
Accepted 14 December 2014
Available online 27 December 2014

Keywords:
Chlorophyll
CO_2 photoreduction
N-doped TiO_2
Spirulina
Visible light

ABSTRACT

The combination of TiO_2 nanoparticles and chlorophyll molecules is promising to provide potential new composite materials for improving photocatalytic CO_2 reduction by merging the ability and features of both material types. In this research, the visible light reactive N-doped TiO_2 (N–TiO_2) catalysts were synthesized using a simple sol–gel method, and chlorophyll in *Spirulina* was consequently loaded onto the N-doped TiO_2 catalysts (Sp/N–TiO_2) in an attempt to enhance the photocatalytic efficiency. The effects of nitrogen and chlorophyll in *Spirulina*, and their loading amount on CO_2 photoreduction with water under visible light of Sp/N–TiO_2 catalysts were investigated. The activities of catalysts were in the order undoped TiO_2 < N–TiO_2 < Sp/N–TiO_2. The addition of *Spirulina* was found to significantly improve the photocatalytic stability and C_{2+} (C_2H_4 and C_2H_6) product selectivity. The 0.5Sp/10N–TiO_2 catalyst exhibited approximately 21.3 times and 1.9 times higher total production yield compared with undoped TiO_2 and 10N–TiO_2, respectively. This outstanding photocatalytic activity could be attributed to the enhancement in visible light harvesting, the surface oxygen vacancies (V_O) facilitating reactants adsorption and dissociation, and the synergistic effect between N–TiO_2 and chlorophyll in *Spirulina*.

1. Introduction

As the recent world population growth in parallel with human overconsumption has increased dramatically, the consumption of energy is therefore expanding at the rate that cannot be acquired [1,2]. This high demand of energy implies an unsustainable development that causes environmental problems due to the increase of greenhouse gas (GHG) emission, especially carbon dioxide (CO_2), which is the main factor responsible of global warming [3–7]. In order to lessen this problem, the balance between conventional energy and alternative energy supplies is essential [8].

Solar energy is one of the largest sustainable and clean energy sources that plays an important role in solving environmental problems. Bacteria, algae, and plants have directly utilized solar energy together with CO_2 to produce their sources of energy over billions of years through photosynthesis [9–11]. During photosynthesis, chlorophyll a as a major photosynthetic pigment plays an essential role in energy absorption from visible light in the range of red and blue lights. Other accessory pigments absorb light in other ranges and conduct energy to the reaction center chlorophyll a by resonance transfer through rings and double bonds in pigment structure [12]. Since photosynthesis is proven to be able to reduce global warming problem and simultaneously offers an energy source, many researchers have investigated the artificial photosynthesis over photocatalysts with the purpose of transforming CO_2 into renewable fuels and environmentally-friendly chemical compounds or green products [13,14].

Among all photocatalysts, titanium oxide (TiO_2) is known to be a promising candidate for photocatalytic CO_2 reduction as regards its superior charge transport property, nontoxicity, and chemical stability [13,15]. The challenge in using TiO_2 is that it is activated mainly within the UV light region due to its wide band gap, leading to a significantly low in utilizing solar energy [16–18]. Doping of a nonmetal (i.e., C, N, S, B, and I) into the TiO_2 lattice is one of the key adopted strategies to expand the adsorption wavelength range to the visible light region [19–23]. The simplest and most practical

* Corresponding author at: Department of Chemical Engineering, Faculty of Engineering, Kasetsart University, Bangkok 10900, Thailand. Tel.: +66 2797 0999; fax: +66 2561 4621.
E-mail address: fengmtc@ku.ac.th (M. Chareonpanich).

http://dx.doi.org/10.1016/j.apcatb.2014.12.022
0926-3373/

modification based on this method is a nitrogen doping according to the band gap narrowing. Nitrogen dopants can result in the species acting as a substitutional nitrogen which generates N 2p states just above valence band maxima or interstitial nitrogen which forms impurity energy level hybridized by N 2p states interacting with O 2p states [24,25]. Moreover, Valentin et al. [26,27] proposed that the presence of nitrogen dopants facilitated the formation of oxygen vacancies (V_O) by reducing the formation energy of V_O from 4.2 to 0.6 eV. However, photocatalytic CO_2 reduction still has major drawbacks in low conversion efficiency. The main reasons are rapid recombination of photogenerated electron–hole pairs, backward reaction, and uncontrolled product selectivity which result in the production of undesired products that cause environmental problems [28–30]. Several modification strategies have been explored to improve the efficiency of CO_2 reduction [31–37], however they are effective to only a limited extent. Inspired by the effective role of chlorophyll in natural photosynthesis, the idea of using chlorophyll in combination with photocatalysts in CO_2 reduction to overcome or lessen the above-mentioned barriers has been evolved in this study.

There have been few literature reviews on the utilization of natural chlorophyll as a novel sensitizer over different catalytic materials. While chlorophyll-modified Pt/KTa(Zr)O_3 and chlorophyll-Cu modified ZrO_2 for enhancing water splitting reaction [38,39], and chlorophyll modified MCM-41 and ZnO for increasing dye degradations under UV–vis irradiation [40,41] have been reported, to our knowledge, chlorophyll modified photocatalyst for photocatalytic CO_2 reduction has been reported only once in the literature in which a single amount of chlorophyll in light-harvesting complex (LHCII) modified Rh-doped TiO_2 was used as the catalyst [42]. The remarkable enhancement of products such as carbon monoxide (CO), acetaldehyde (CH_3CHO), and methyl formate (CH_3OCHO) was obtained from CO_2 reduction with water compared to the unmodified catalyst. The role of chlorophyll in photocatalytic CO_2 reduction is not clear to date. Hence, it is certainly interesting to further examine the junction effect between chlorophyll and photocatalyst, amounts of chlorophyll loading to exploit the maximum ability, and especially the mechanism of chlorophyll-modified catalysts in CO_2 photoreduction.

Among all the photosynthetic species found in nature, *S. platensis* appears to have one of the highest chlorophyll contents, approximately 1.15% of its biomass [43,44]. The uses of chlorophyll in *S. platensis* is a potential alternative to enhance the photocatalytic activity due to its high chlorophyll contents and ease of cultivation [45]. Accordingly, in this work, *Spirulina*-modified N-doped TiO_2 catalysts have been proposed with an attempt to improve the efficiency and stability in photocatalytic CO_2 reduction to green products under visible light. The roles of nitrogen, chlorophyll in *Spirulina*, and their loading amounts in CO_2 reduction have been investigated in detail. It was found that chlorophyll in *Spirulina* could significantly increase the photocatalytic stability and promote the response for chain growth probability of hydrocarbon products. The mechanism of CO_2 photoreduction with water on *Spirulina*-modified N-doped TiO_2 has been proposed.

2. Experimental

2.1. Synthesis of Spirulina-modified N-doped TiO_2 catalysts

A two-step process was used to prepare *Spirulina*-modified N-doped TiO_2 catalysts. The first step was the synthesis of N-doped TiO_2 through a sol–gel method modified from the work reported by Collazzo et al. [46]. In this work, titanium (IV) isopropoxide ($Ti(OCH(CH_3)_2)_4$: Aldrich, >97% purity) was used as a TiO_2 precursor. A certain volume of ammonia solution (QReC, 28% w/w) was added dropwise into titanium (IV) isopropoxide solution at a rate of 1 ml min^{-1} to initiate the hydrolysis process, and then the obtained mixture was vigorously stirred for 30 min. After that, the mixture was dried at 100 °C for 2 h and calcined in air at 400 °C for 2 h with a heating rate of 2 °C min^{-1}. The yellow powder catalyst was obtained. The nitrogen concentrations based on titanium in the catalyst were varied in the range of 5–15 wt% N. The second step was the modification of N-doped TiO_2 by commercial *Spirulina* using incipient wetness impregnation method. Briefly, *Spirulina* pellets (the biological and chemical composition of *Spirulina* are shown in Table S1) were ground and dissolved in deionized water and then added onto N–TiO_2 catalyst. The loading amount of *Spirulina* was based on chlorophyll a in *Spirulina*, which can be calculated from Eq. (1) [47]:

$$\text{Chlorophyll a} = 9.78A_{663} - 0.99A_{645}(\text{mgl}^{-1}) \quad (1)$$

where A_{645} and A_{663} are absorbances at 645 and 663 nm, respectively, measured by using a UV–vis spectrophotometer. The obtained mixture was continuously stirred at 40 °C overnight until water was completely evaporated. The percentages of chlorophyll a in *Spirulina*-modified TiO_2 catalysts used in this study were 0.1, 0.5, and 1.0 wt%. The obtained catalysts was labeled as *x*Sp/*y*N–TiO_2, where *x* and *y* are the weight percentages of chlorophyll a in *Spirulina* and nitrogen, respectively. For comparison, the undoped TiO_2 was also prepared by titanium (IV) isopropoxide hydrolysis with deionized water using the same procedure as that of N-doped catalyst.

2.2. Catalyst characterization

Nitrogen sorption isotherms of the catalysts were measured at −196 °C using a Quantachrome Autosorp-1C instrument. Prior to sorption measurements, the catalysts were degassed at 200 °C. The specific surface area of the catalysts was obtained by using Brunauer–Emmert–Teller (BET) analysis in the relative pressure (P/P_0) range between 0.05 and 0.3. Pore size distribution was calculated by using Barrett–Joyner–Halenda (BJH) method. The specific pore volumes were measured at a relative pressure of 0.995.

The crystalline phase of TiO_2 catalysts was analyzed by X-ray diffraction spectroscopy (XRD: Bruker D8 Advance) operated with monochromated Cu Kα radiation (40 kV to 40 mA) at room temperature. TiO_2 crystallite size was calculated by means of the Scherrer equation.

The morphology, size, and lattice structure of the catalysts were examined by using high-resolution transmission electron microscopy (HR-TEM: JEOL JEM-2010 instrument) with an acceleration voltage of 200 kV.

Field emission scanning electron microscopy (FE-SEM: JEOL, JSM-7600F) with energy dispersive X-ray spectroscopy (EDS: OXFORD, X-Max^N) operated at 15 keV with Pt-coated was performed to examine the catalyst morphologies and to map surface elements of the catalysts.

The functional groups of the catalysts were examined by using Fourier transform infrared spectroscopy (FT-IR: Bruker TENSOR 27) equipped with a DTGS detector in the range of 4000–400 cm^{-1}.

The optical property and band gap energy of the catalysts were recorded with UV–vis diffuse reflectance spectroscopy (UV–vis DRS: JASCO, V-670) using $BaSO_4$ as a reflectance standard. To obtain the band gap energy, the original reflectance spectra were transformed to the plot of $(\alpha h\nu)^{1/2}$ as a function of photon energy ($h\nu$) to be in accordance with the theoretical equation as shown below:

$$\alpha h\nu = A(h\nu - E_g)^2 \quad (2)$$

where α is the absorption coefficient, A is a constant, and E_g is the band gap energy. The band gap energy was determined from the

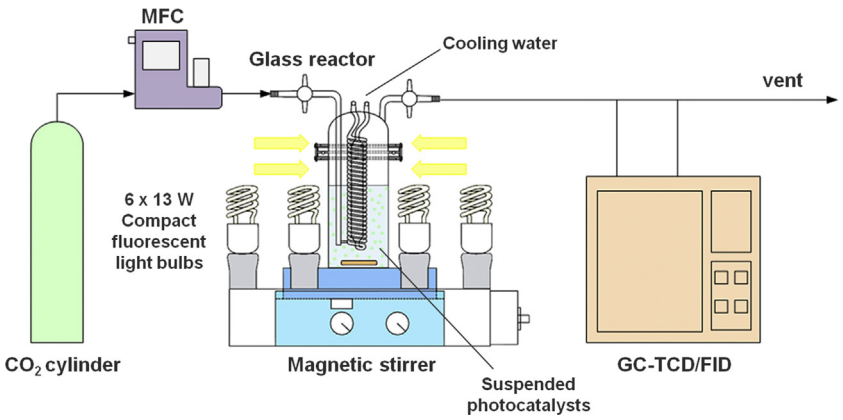

Fig. 1. Schematic of experimental system for CO_2 photoreduction.

cross point of the tangent line through the maximum slope with its lower curve baseline.

X-ray photoelectron spectroscopy (XPS), carried out at beamline 3.2a of the synchrotron light research institute (SLRI), Thailand, was used to identify the surface atomic concentrations and chemical states of the catalysts. The photoelectron spectra were collected through a Thermo VG Scientific Alpha110 energy analyzer with the maximum photon energy of 600 eV and the energy step of 0.1 eV. The C 1s peak at 284.6 eV was used as a reference peak for all binding energies.

Photoluminescence spectroscopy (PL: AvaSpec-2048TEC, Avantes) was carried out at room temperature in the range of 300–700 nm using an excitation wavelength of 255 nm to examine the charge transfer process of catalysts.

The local geometry of Ti in the modified-TiO_2 catalysts was examined by using X-ray absorption near-edge structure (XANES) at beamline 8 of the SLRI, Thailand. A Ge (220) double crystal monochromator was used for photon energy selection. XANES spectra were recorded at room temperature in the transmission mode using ionization chambers with the energy range of 4940–5050 eV and the step of 0.2 eV. Titanium metallic foil was used for calibration at the Ti k-edge at 4966 eV. The obtained spectra were corrected for background absorptions and normalized by Athena program.

2.3. CO_2 photoreduction activity measurements

The experiments on CO_2 photoreduction with water over the modified TiO_2 catalysts were carried out in a photoreactor system as shown in Fig. 1. The compact fluorescent integrated bulbs (Philips Tornado: 6 bulbs, 13 watt) located around a continuous flow stirred slurry reactor (CFSSR) were used as the visible light source. The light intensity at the catalyst zone was approximately 0.37 ± 0.05 mW cm^{-2}, and wavelengths were in the range of 400–800 nm. Prior to experiment, 0.25 g of each catalyst was loaded into the CFSSR which contained 250 ml distilled water. The catalyst concentration was fixed as 1 g–dm^{-3} to avoid the effect of light scattering and achieve the maximum ability of light to reach every catalyst particle [28,48,49]. A magnetic stirrer placed at the bottom of the reactor vessel helped to generate a continuously-stirred slurry system, resulting in the uniform distribution of catalyst particles in the slurry. CO_2 (>99.9% purity) was continuously introduced into the CFSSR by using a mass flow controller at a flow rate of 60 ml min^{-1} for 1 h to purge air and saturate the solution. After that, the flow rate of CO_2 was decreased and maintained at 10 ml min^{-1} throughout the experiment. The photocatalytic reaction was started by turned on the light from the compact fluorescent integrated bulbs, and irradiation was continued for 6 h. The effluent gaseous products were analyzed by using a Shimadzu GC-2014 gas chromatograph equipped with a thermal conductivity detector (TCD) and a Unibead-C column for H_2, CO, CO_2, and CH_4 analysis, as well as a Shimadzu GC-8A gas chromatograph equipped with a flame ionization detector (FID) and a Porapak-Q column for hydrocarbon analysis.

3. Results and discussion

3.1. Crystal structure and textural property of modified TiO_2 catalysts

The XRD patterns at 2θ of 25.3° and the normalized Ti L-edge XANES spectra shown in Fig. 2 and Fig. S1, respectively, evidently confirmed the existence of anatase phase of all catalysts. For N-doped TiO_2 catalysts, the peak intensities increased compared to that of undoped TiO_2; this indicated that nitrogen dopants could enhance the crystallinity of TiO_2 particles. However, the amount of nitrogen dopants was not enough to cause a structural phase transition. For *Spirulina*-modified TiO_2 catalysts (Fig. 2e–g), the diffraction peaks were similar to that of N-doped TiO_2 catalyst (Fig. 2c). It should be noted that the heavy metal in *Spirulina* was not observed by XRD due to its trace amount in *Spirulina*. The TiO_2 crystallite sizes estimated from XRD patterns by using the Scherrer equation are listed in Table 1. The crystallite sizes of modified TiO_2 catalysts were increased with increasing amounts of nitrogen

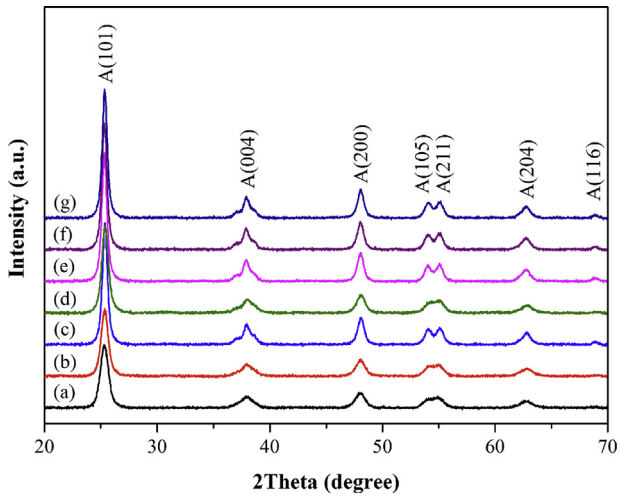

Fig. 2. XRD patterns of (a) TiO_2, (b) 5N–TiO_2, (c) 10N–TiO_2, (d) 15N–TiO_2, (e) 0.1Sp/10N–TiO_2, (f) 0.5Sp/10N–TiO_2, and (g) 1.0Sp/10N–TiO_2 catalysts (A = anatase).

Table 1
Crystallite size, BET surface area, pore volume, pore size, and band gap of TiO_2 and modified TiO_2 catalysts.

Catalysts	Crystallite size[a] (nm)	Specific surface area (m^2/g)	Total pore volume (cm^3/g)	Pore size (nm)	Band gap (eV)	
					E_{g1}	E_{g2}
TiO_2	9.6	114	0.35	48.9	3.09	–
5N–TiO_2	11.0	102	0.32	48.9	3.08	2.42
10N–TiO_2	14.9	86	0.35	55.7	3.06	2.18
15N–TiO_2	11.5	107	0.34	52.5	3.07	2.25
0.1Sp/10N–TiO_2	15.6	81	0.28	56.0	3.05	n/a
0.5Sp/10N–TiO_2	15.3	68	0.38	56.0	3.03	n/a
1.0Sp/10N–TiO_2	15.8	59	0.21	48.9	3.01	n/a

n/a: not applicable.
[a] Calculated from the Scherrer equation.

dopants (as will be reported later in inset of Fig. 8A), as 10N–TiO_2 catalyst exhibited the largest crystallite size (14.9 nm). However, the crystallite size was hardly changed after *Spirulina* loading.

Pore characteristics of undoped TiO_2 and modified TiO_2 catalysts analyzed by nitrogen sorption technique are shown in Fig. 3, and the specific surface area, total pore volume, and pore size are listed in Table 1. All the isotherms in Fig. 3A show the typical structure of type IV isotherm with well-defined H1 hysteresis loop, indicating the characteristic of capillary condensation within uniform mesoporous structures [50]. These results confirmed that the mesoporous structures were well retained after nitrogen doping and *Spirulina* loading. The mean pore sizes of TiO_2 catalysts, as shown in Fig. 3B and Table 1, were slightly increased with increasing amounts of nitrogen dopants (Fig. 3B: c and d), while they were decreased with increasing amounts of *Spirulina* loading (Fig. 3B: g). The specific surface area and total pore volume of undoped TiO_2 catalyst were 114 m^2/g and 0.35 cm^3/g, respectively.

With increasing amounts of nitrogen dopant, a decrease in the specific surface area was observed, while the total pore volume was unchanged. Similar decreases in surface area of N-doped TiO_2 were also observed by Liu and Syu [51] and Gurkan et al. [52]. This could be attributed to the higher crystallite sizes of N-doped TiO_2 catalysts caused by nitrogen dopants in the form of interstitial N (Ti—O—N or Ti—N—O) or substitutional N (Ti—N), since N^{3-} ion has a larger ionic radius (0.171 nm) than that of O^{2-} ion (0.140 nm) [53].

Moreover, the specific surface areas of the catalysts were significantly decreased by 1.1 to 1.5 times when the loading of chlorophyll in *Spirulina* was increased from 0.1 to 1.0 wt% chl a. A similar trend was observed with the total pore volume of *Spirulina*-modified

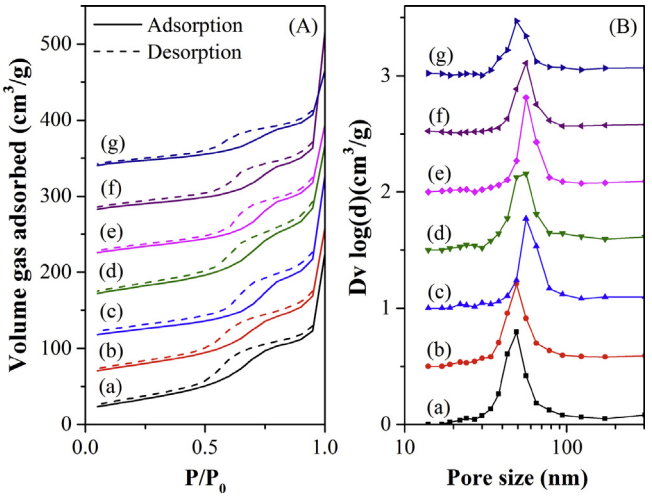

Fig. 3. (A) Nitrogen adsorption–desorption isotherm and (B) pore size distribution of TiO_2 and modified TiO_2 catalysts: (a) TiO_2, (b) 5N–TiO_2, (c) 10N–TiO_2, (d) 15N–TiO_2, (e) 0.1Sp/10N–TiO_2, (f) 0.5Sp/10N–TiO_2, and (g) 1.0Sp/10N–TiO_2.

TiO_2 catalysts, except that the 0.5Sp/10N–TiO_2 catalyst exhibited the highest total pore volume among all the catalysts (0.38 cm^3/g). The decrease of specific surface area and pore volume of *Spirulina*-modified TiO_2 catalysts was possibly due to the addition of large *Spirulina* particles with nonporous surface (Fig. S2) onto the modified TiO_2 catalysts.

3.2. Morphology and surface characteristics of modified TiO_2 catalysts

Fig. 4 shows TEM and HRTEM images of undoped TiO_2, 10N–TiO_2, and 0.5Sp/10N–TiO_2 catalysts. TEM image of undoped TiO_2 (Fig. 4a) displayed an agglomeration of TiO_2 nanoparticles with the crystallite size in the range of 8–12 nm. The morphologies of 10N–TiO_2 and 0.5Sp/10N–TiO_2 catalysts (Fig. 4c and e) were similar to the undoped TiO_2 catalyst except that the crystallite sizes were in the range of 12–20 nm, which are in good agreement with the average size calculated from the Scherrer equation. In addition, the presence of *Spirulina* was not observed in the TEM image of 0.5Sp/10N–TiO_2 catalyst, as shown in Fig. 4e (TEM images of pure *Spirulina* are shown in Fig. S2a and b). The HRTEM images (Fig. 4b, d, and f) exhibited clear lattice fringes within individual nanocrystals, with interplanar spacings of 0.350 and 0.243 nm, corresponding to (1 0 1) and (1 0 3) planes of anatase in accordance with the XRD results [54,55], respectively.

The apparent morphologies of undoped TiO_2, 10N–TiO_2, and 0.5Sp/10N–TiO_2 catalysts were further examined by FE-SEM as shown in Fig. 5. Without nitrogen dopants, it was observed that tiny and uniform TiO_2 nanoparticles (Fig. 5a) agglomerated into an irregular spherical shape. The interparticle mesopores created between closely packed particles were clearly seen in the inset of Fig. 5a. A higher degree of particle aggregation was found in the case of 10N–TiO_2 catalyst (Fig. 5b), and mesopores with larger pore size than that of undoped TiO_2 resulted from assemble particles were evidently observed (inset of Fig. 5b). In the case of 0.5Sp/10N–TiO_2 catalyst (Fig. 5c), *Spirulina* was partially covered by N-doped TiO_2 (SEM images of pure *Spirulina* are shown in Fig. S2c and d). It should be noted that the surface of *Spirulina*-modified TiO_2 catalyst was rougher than that of N-doped TiO_2 catalyst (Fig. 5b) due to the fact that some of chlorophylls or other compounds in *Spirulina* might dissolve in water and disperse on N-doped TiO_2 catalyst. FE-SEM/EDS mapping images of 0.5Sp/10N–TiO_2 catalyst in Fig. S3 also exhibited the well dispersions of C, O, N, and Mg atoms in chlorophyll on the catalyst.

The functional groups of undoped TiO_2 and modified TiO_2 catalysts were examined by using FT-IR spectroscopy (Fig. 6). All catalysts (Fig. 6a–c) displayed the typical features of TiO_2, including O—H stretching mode of Ti—OH on TiO_2 surface and water molecules at 3406 cm^{-1}, O—H bending mode of hydroxyl group on Ti—OH and water molecules at 1624 cm^{-1}, and broad peak O—Ti—O stretching adsorption band around 800–400 cm^{-1}. Comparing to the spectral profile of undoped TiO_2, 10N–TiO_2

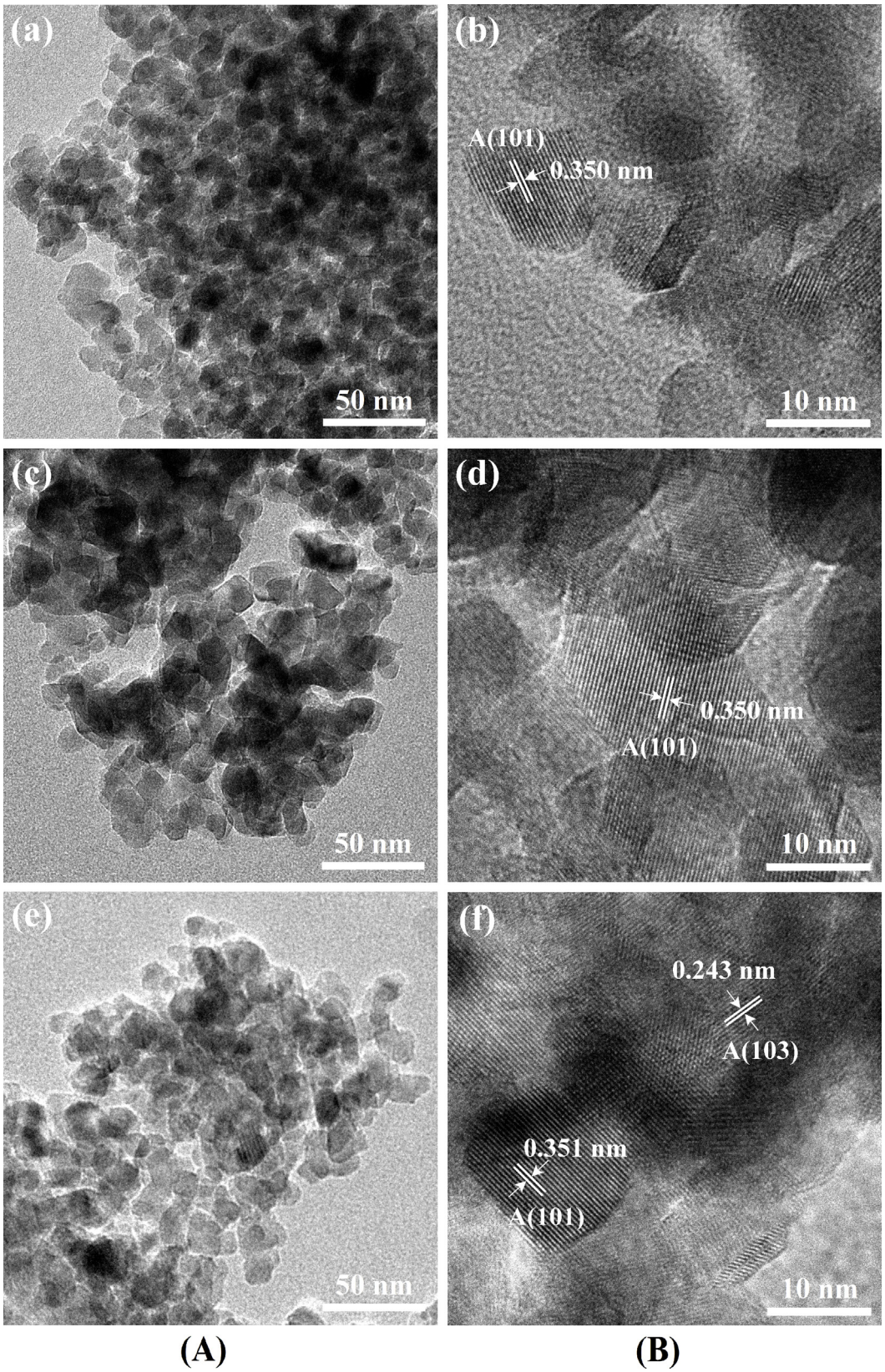

Fig. 4. TEM (A) and HRTEM (B) images of TiO_2 (a, b), 10N–TiO2 (c, d), and 0.5Sp/10N–TiO_2 (e, f) catalysts (A = anatase).

catalyst (Fig. 6b) shows the small peak at 1380 cm^{-1}, corresponding to the species containing CN bonds or nitrogen oxide species [56]. In addition, 0.5Sp/10N–TiO_2 catalyst (Fig. 6c) shows the peaks originating from CH stretching of methyl, methylene or methine group at 2920 cm^{-1}, C=O stretching in conjugated ketone and carbonyl groups at 1655 cm^{-1}, and C=N stretching in chlorophyll around 1540 cm^{-1} [57,58], similar to *Spirulina* spectra (Fig. 6d). Accordingly, these observations

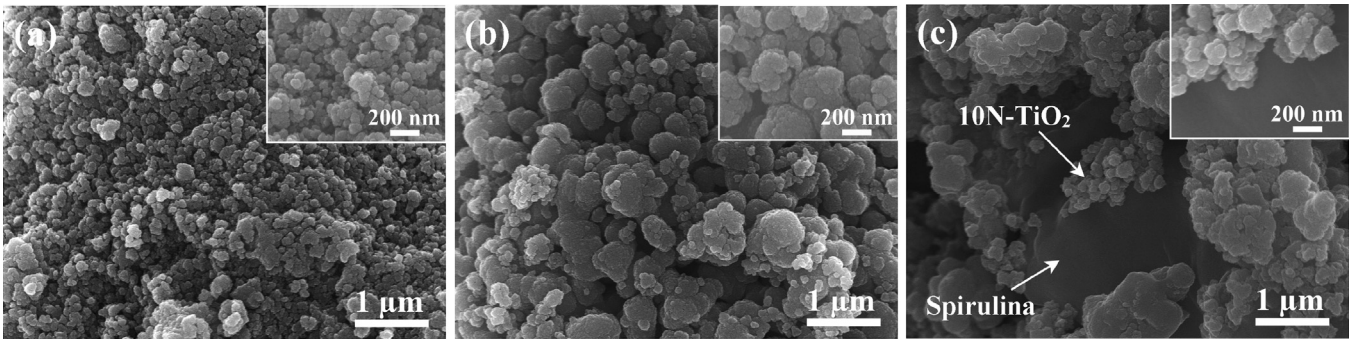

Fig. 5. FE-SEM images of (a) TiO_2, (b) 10N–TiO_2, and (c) 0.5Sp/10N–TiO_2 catalysts.

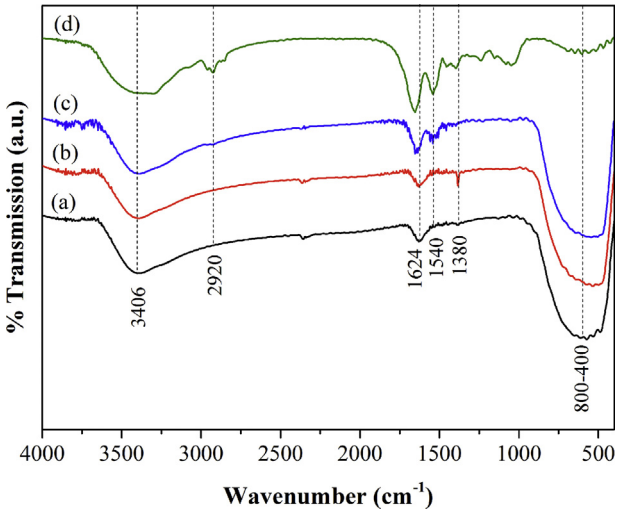

Fig. 6. FT-IR spectra of (a) TiO_2, (b) 10N–TiO_2, (c) 0.5Sp/N–TiO_2 catalysts, and (d) *Spirulina*.

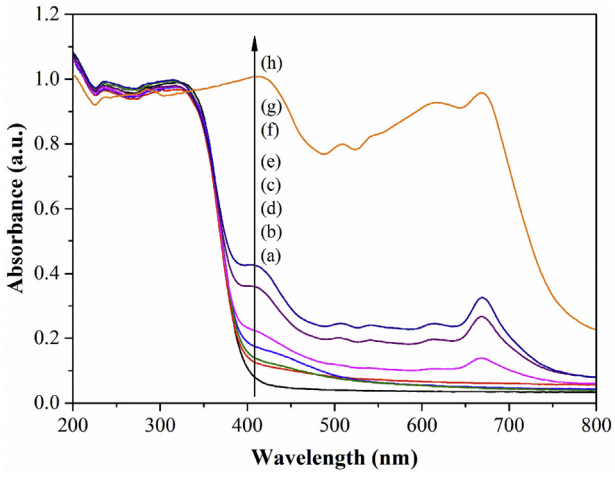

Fig. 7. UV–vis diffuse reflectance spectra of TiO_2 and modified TiO_2 catalysts: (a) TiO_2, (b) 5N–TiO_2, (c) 10N–TiO_2, (d) 15N–TiO_2, (e) 0.1Sp/10N–TiO_2, (f) 0.5Sp/10N–TiO_2, (g) 1.0Sp/10N–TiO_2, and (h) *Spirulina*.

clearly confirm the presence of chlorophyll in the *Spirulina*-modified TiO_2 catalysts.

3.3. Optical property and band gap energy of modified TiO_2 catalysts

UV–vis diffuse reflectance spectra of undoped TiO_2 and modified TiO_2 catalysts are shown in Fig. 7. The undoped TiO_2 catalyst exhibited absorption only in the UV region with the absorption edge around 400 nm. For the N-doped TiO_2 catalysts (Fig. 7b–d), the absorptions were extended to the visible region. The band gap energies (E_{g1}) of the N-doped TiO_2 catalysts listed in Table 1 were slightly narrower than that of the undoped TiO_2 (3.09 eV). Sub-band gap energies (E_{g2}) related to impurity energy level of continuous N—O states above the maximum valence band of O 2p valence were observed in N-doped TiO_2 catalysts, which is similar to the results reported by Shao et al. [59] and Li et al. [60]. Among all the N-doped TiO_2 catalysts, 10N–TiO_2 (Fig. 7c) exhibited the highest visible light absorption in the range of 400–500 nm with the lowest sub-band gap energy of 2.18 eV. This sub-band gap energy consequently led to the visible light response [61,62]. The *Spirulina*-modified TiO_2 catalysts (Fig. 7e–g) had strong absorption capacity in the visible light region (400–800 nm), corresponding to the characteristic absorption pattern of *Spirulina* (Fig. 7h). The broad absorption bands around 400–500 and 600–750 nm originating from chlorophyll could harvest visible light and create a color center [63]. As a result, the visible light absorption capacity of catalysts was increased, while the band gap energy (in Table 1) was slightly decreased with increasing *Spirulina* loading.

3.4. Chemical state of modified TiO_2 catalysts

The electronic properties and bonding of nitrogen dopants of the undoped and N-doped TiO_2 catalysts were examined through N 1s core level spectra of XPS technique. As shown in Fig. 8A, the undoped TiO_2 rarely shows any peaks of N 1s, while N-doped TiO_2 catalysts exhibited broad peak centered at 399.8 eV (for 5N–TiO_2), 399.8 eV (for 10N–TiO_2), and 400.6 eV (for 15N–TiO_2). In the case of 5N–TiO_2 and 10N–TiO_2 catalysts, the peaks observed were attributed to a N atom replacing an O atom in the TiO_2 crystal lattice to form the Ti—N—O linkage [64,65]. A higher intensity peak was observed from 10N–TiO_2, indicating an increase in the electron density of N atom upon nitrogen dopants in the TiO_2 lattice. In the case of 15N–TiO_2, the N 1s peak was 0.8 eV shifted to higher binding energy; this might be due to the signals of the absorbed molecular nitrogen species (N_2) or nitroxide species (e.g., NO and NO_2) (≥400.3 eV) [66]. After background subtraction and curve fitting, the amounts of N dopants (inset of Fig. 8A) were calculated from the areas of Ti 2p, N 1s, and O 1s photoemission peaks and weighted by the atomic sensitivity factors of each atomic level. It was found that approximately 2.91 at.% of nitrogen was successfully doped onto the 10N–TiO_2 catalyst. The amounts of nitrogen dopants on the catalysts were in good agreement with the increase in the visible light absorption capacity observed from the UV–DRS result.

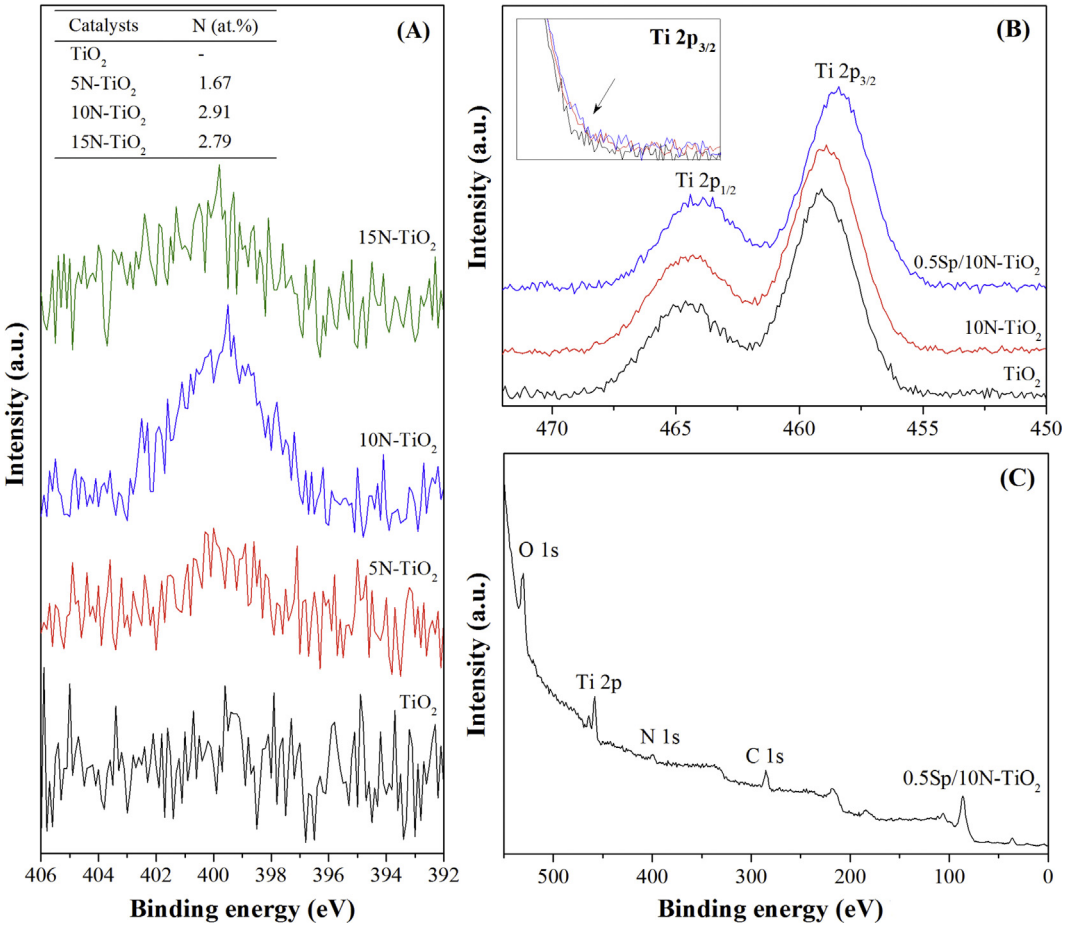

Fig. 8. High resolution XPS spectra of (A) N 1s, (B) Ti 2p of TiO_2 and modified TiO_2 catalysts, and (C) survey spectrum of 0.5Sp/10N–TiO_2 catalyst.

Fig. 8B shows XPS spectra of Ti 2p core levels of undoped TiO_2 and modified TiO_2 catalysts. The respective spin orbits of Ti $2p_{3/2}$ and Ti $2p_{1/2}$ were clearly seen in all Ti 2p spectra, this indicated that the oxidation state of titanium atoms in the catalysts were in the form of Ti^{4+}. The binding energy of Ti $2p_{3/2}$ in 10N–TiO_2 (458.9 eV) and 0.5Sp/10N–TiO_2 catalysts (458.6 eV) were lower than that of undoped TiO_2 (459.2 eV), indicating an increase in the electron density around titanium atoms. This result confirmed the presence of N atoms in the form of interstitial N in TiO_2 lattice due to the fact that the electronegativity of nitrogen is less than that of oxygen [24]. Compared with the undoped TiO_2 spectrum (inset of Fig. 8B), the spectra of N-doped and *Spirulina*-modified TiO_2 exhibited a shoulder at the lower band gap energy of Ti $2p_{3/2}$, which were ascribed to Ti^{3+} oxidation state [67]. This indicated the occurrence of V_O on the surface of TiO_2 catalysts [68].

The survey spectrum of 0.5Sp/10N–TiO_2 catalyst in Fig. 8C obviously indicated the characteristic peaks of Ti 2p, O 1s, and C 1s together with a small peak of N 1s. In the case of the *Spirulina*-modified TiO_2 catalysts, the amounts of hydroxyl group or chemisorbed oxygen, nitrogen, and carbon observed on the surface of the catalysts were greater than those of the undoped and N-doped TiO_2 catalysts and were increased with the loading percentages of chlorophyll a in *Spirulina*. This indicated that *Spirulina* on the catalysts could be exposed to light irradiation, confirming the appearance of *Spirulina* in SEM result (Fig. 5c). However, the peaks of other metals in *Spirulina* were not found due to their trace amounts in *Spirulina*.

3.5. Photocatalytic activity of modified TiO_2 catalysts

Prior to each experiment, blank tests were performed to ensure that the products were originated from photocatalytic reaction. The results show that without photocatalyst or visible light irradiation, no H_2 and hydrocarbon products were observed. Moreover, when the photocatalyst was replaced by pure *Spirulina* with the presences of CO_2 and water in the reactor, no products were detected under visible light irradiation. This result confirmed that *Spirulina* alone could not function as a photocatalyst.

The performances of undoped and N-doped TiO_2 catalysts in photocatalytic CO_2 reduction were tested in order to investigate the effect of nitrogen doping on photocatalysts, and the H_2 production as a function of irradiation time is shown in Fig. 9A. Undoped TiO_2 catalyst rarely shows activity under visible light irradiation, which corresponds well with the inability of visible light absorption shown in Fig. 7. In contrast, all N-doped TiO_2 catalysts demonstrated higher H_2 production than that of undoped TiO_2 despite of their lower specific surface areas. This enhancement could be attributed to nitrogen dopants and V_O in the N-doped catalysts. Nitrogen dopants in a form of interstitial N species (as was confirmed by N 1s of the XPS results) were proposed to create impurity energy levels of N—O unit above TiO_2 valence band [17,25,68]. Accordingly, Peng et al. [69] reported that the highest impurity energy level of interstitial N above the TiO_2 maximum valence band (0.73 eV) was more favorable for visible light response than that of the substitutional N (0.14 eV). Meanwhile V_O formed on the surface was considered to be active adsorption sites for

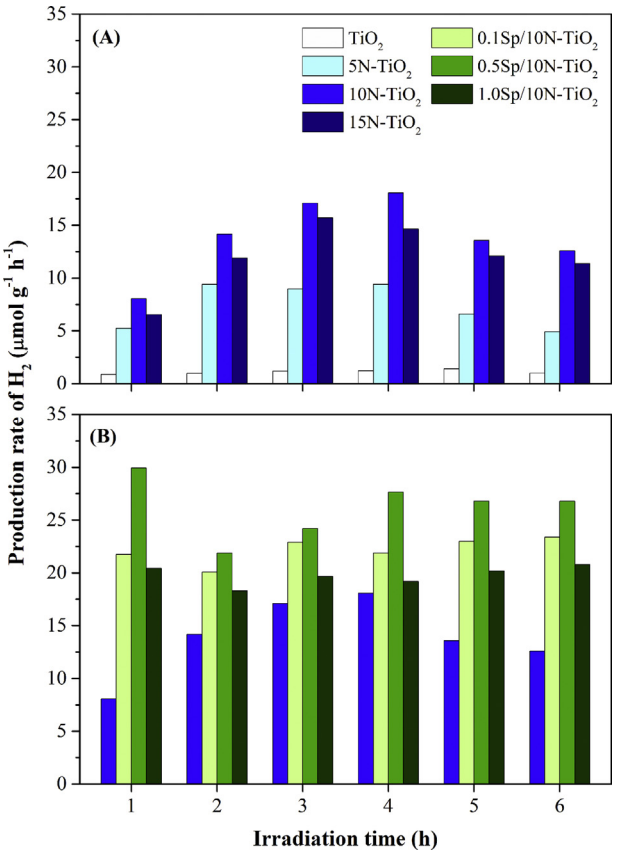

Fig. 9. Production rate of H_2 as a function of irradiation time over TiO_2 and modified TiO_2 catalysts.

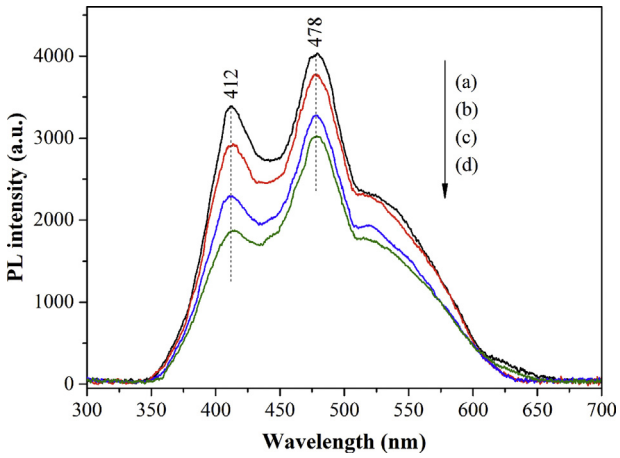

Fig. 10. PL spectra of (a) 10N–TiO_2, (b) 0.1Sp/10N–TiO_2, (c) 0.5Sp/10N–TiO_2, and (d) 1.0Sp/10N–TiO_2 catalysts (excitation at 255 nm).

H_2O and CO_2, and hence enhanced the visible light harvesting [70,71].

As shown in Fig. 9A, amounts of H_2 products were decreased after 4–5 h time on stream of photoreaction, indicating the gradual deactivation of catalysts; similar observation was reported elsewhere in the literature [49,72]. The possible reasons of deactivation are the saturation of adsorption sites on TiO_2 surface by intermediate products or backward reaction that potentially converts some products to intermediates and reactants [49,73,74]. It was found that H_2 production of N-doped catalysts followed the order 5N–TiO_2 < 15N–TiO_2 < 10N–TiO_2. This was likely due to the lowest band gap energy, the highest visible light response as well as surface nitrogen concentration of 10N–TiO_2, as confirmed by UV–vis DRS and XPS analyses in Fig. 7 and the inset of Fig. 8A.

To further examine the effect of chlorophyll in *Spirulina* on photocatalytic performance, TiO_2 with the optimum nitrogen doping amount (10N–TiO_2) was selected to load various concentrations of chlorophyll in *Spirulina* (0.1, 0.5 and 1.0 wt% chl a). From the amount of H_2 production as shown in Fig. 9B, all *Spirulina*-modified TiO_2 catalysts could notably enhance the activity of 10N–TiO_2 catalyst. The maximum H_2 production of 29.93 $\mu mol\, g^{-1}\, h^{-1}$ was obtained from 0.5Sp/10N–TiO_2 catalyst at time on stream of 1 h. A possible reason is that high *Spirulina* loading (1.0 wt%) causes significant decrease in the specific surface area of catalysts, as shown in Table 1. In addition, this high loading might lead to the formation of recombination centers due to large population of photo-induced electron–hole pairs [31,60,75]. In terms of catalyst stability, the *Spirulina*-modified TiO_2 catalysts exhibited higher H_2 production at early reaction stage, and then appeared to remain constant for the rest of irradiation times, indicating longer-term stability compared to those of N-doped TiO_2 catalysts.

All these results indicated that chlorophyll in *Spirulina* had an important role in photocatalytic activity. As mentioned in the result of UV–vis DRS, *Spirulina*-modified TiO_2 catalysts show high absorption of photons with different wavelengths in the visible light regime, these photons could excite electrons in chlorophyll to excited states. In order to clarify the photoexcited electron transfer process between 10N–TiO_2 catalyst and chlorophyll in *Spirulina*, PL spectroscopy was performed and PL spectra as shown in Fig. 10 exhibited the broad PL emission band with peaks at 412 and 478 nm for all catalysts. It was found that PL intensities of 10N–TiO_2 catalysts were decreased with *Spirulina* loading, indicating the efficient contact and occurrence of the charge transfer between 10N–TiO_2 catalyst and chlorophyll in *Spirulina* [38]. Since both of 10N–TiO_2 catalyst and chlorophyll in *Spirulina* can absorb the light in UV region (as shown in Fig. 7c and h), the direction of the charge transfers then need to be confirmed by the energy levels of 10N–TiO_2 catalyst and chlorophyll in *Spirulina*. Accordingly, Kathiravan et al. [76] reported that the oxidation potential of excited state of chlorophyll is −1.27 vs. SCE, while the conduction band potential of TiO_2 is −0.1 vs. SCE. Based on these information, electrons then transferred from excited state of chlorophyll to the conduction band of 10N–TiO_2 due to the energetically higher excited states of chlorophyll. In addition, the PL intensities of 10N–TiO_2 catalysts were continuously decreased with the increase in *Spirulina* loading, suggesting the higher degree of electron transfer with respect to chlorophyll contents. Furthermore, the electron transfer from excited state of chlorophyll to the conduction band of TiO_2 was also confirmed by Kathiravan et al. [76] using fluorescence lifetime measurement since the chlorophyll adsorbed on TiO_2 had the shorter fluorescence lifetime than that of the unadsorbed TiO_2. There have been few literature [40,41] proposed on the electron transfer process from pure chlorophyll to photocatalysts as well. Therefore, chlorophyll in *Spirulina* could potentially act as a photosensitizer or electron donor, and as a result, the additional electrons from chlorophyll help improve the photocatalytic reaction efficiency by reducing more adsorbed molecules, such as CO_2 and other intermediates, on the catalyst surface.

The cumulative productions over TiO_2 and modified TiO_2 catalysts for the time on stream of 6 h were calculated by integrating the production rate with irradiation time, and the results are summarized in Table 2. It was found that the cumulative H_2 production over 10N–TiO_2 and 0.5Sp/10N–TiO_2 catalysts were approximately 12 times and 22 times higher than that of undoped TiO_2, respectively. Similar to those reported elsewhere [77–80], besides H_2, C_2H_4 and C_2H_6 as the desired products, as well as CH_4 as the undesired product, were also detected in this work. The

Table 2
Amounts of photoreduction products, product selectivity, and quantum yield under visible light irradiation for 6 h.

Catalysts	Production yield (μmol g^{-1})					Selectivity[a]	Φ_{total}[b](%)
	H_2	CH_4	C_2H_4	C_2H_6	Total		
TiO_2	6.54	0.27	–	0.02	6.83	0.08	0.005
5N–TiO_2	42.43	0.78	0.03	0.04	43.28	0.09	0.015
10N–TiO_2	77.66	0.93	0.05	0.07	78.10	0.13	0.025
15N–TiO_2	67.06	0.80	0.04	0.06	67.97	0.13	0.021
0.1Sp/10N–TiO_2	121.82	0.45	0.08	0.17	122.52	0.56	0.054
0.5Sp/10N–TiO_2	144.99	0.48	0.12	0.17	145.76	0.60	0.060
1.0Sp/10N–TiO_2	108.81	0.38	0.07	0.13	109.39	0.53	0.042

[a] Selectivity of CO_2 reduction products is defined as the number of moles of desired products (C_2H_4 and C_2H_6) per the number of moles of undesired product (CH_4).
[b] Φ_{total} is the sum of quantum yield of desired products (C_2H_4 and C_2H_6) from CO_2 reduction.

amounts of products from CO_2 reduction were normally in an order $C_2H_4 < C_2H_6 < CH_4 < H_2$. Since a large amount of H_2 was generated, it is implied that water splitting reaction was more favorable than CO_2 reduction. As previously reported by He et al. [71], the binding energy on the vacant site of H_2O was 0.64 eV higher than that of CO_2, as a result the adsorption of CO_2 could be potentially hindered by H_2O. However, hydrogen was simultaneously consumed during CO_2 reduction to produce hydrocarbon products. As shown in Table 2, the maximum amounts of C_2H_4 and C_2H_6 were obtained from 0.5Sp/10N–TiO_2 catalysts (0.17 and 0.12 μmol g^{-1}, respectively), while the maximum amount of CH_4 was obtained from 10N–TiO_2 catalyst (0.93 μmol g^{-1}).

Considering the product selectivity of CO_2 reduction, the addition of chlorophyll in *Spirulina* could significantly increase the selectivity of the C_{2+} products (C_2H_4 and C_2H_6), which are the green and potentially applicable products. This suggested that the increase in available electrons from chlorophyll in *Spirulina* likely promoted the response for chain growth probability of hydrocarbon products. Among all the catalysts, 0.5Sp/10N–TiO_2 catalyst gave the highest desired product selectivity of 0.60 (Table 2). Moreover, due to the fact that similar products were observed when both N-doped TiO_2 and *Spirulina*-modified TiO_2 catalysts were applied, this evidently implied that the products reported in Table 2 were obtained as the result of CO_2 reduction (not from degradation of *Spirulina* itself).

The photocatalytic activity of 0.5Sp/10N–TiO_2 catalyst for 24 h was carried out in order to study the decomposition of *Spirulina*. As shown in Fig. S4, the rate of H_2 production remains constant at the early reaction stage (1–7 h) and then gradually decreased while the rate of CH_4 production decreased after reaching their maximum values. The decrease in the production rate exhibited a gradual deactivation of the catalyst. The possible reasons of deactivation could be attributed to the saturation of adsorption sites on TiO_2 surface, backward reactions [49,73,74], or the decomposition of *Spirulina* itself.

The FT-IR spectra of 0.5Sp/10N–TiO_2 catalysts (inset of Fig. S5) confirmed the partial decomposition of *Spirulina* during the reaction time since the peak intensities originating from the functional groups of chlorophyll in *Spirulina* of the catalyst after 24-h reaction (Fig. S5b) slightly decreased compared to that of the catalyst before reaction (Fig. S5a). The color of the catalyst after 24-h reaction (Fig. S4) also faded from that of the catalyst before reaction, indicating the decomposition of *Spirulina*. The decomposition of *Spirulina* was further investigated by using UV–vis spectroscopy to examine the reaction solution. As shown in Fig. S5, UV–vis spectrum of the reaction solution collected after 24-h reaction (Fig. S5b) exhibited a higher absorbance intensity around 190–300 nm compared to that of the catalyst before reaction (Fig. S5a). These results demonstrated that decomposed compounds from *Spirulina* could potentially dissolve into the reaction solution.

In order to compare the result of this work to those previously published on the basis of a mole of photon from light irradiation absorbed by the catalyst, the total quantum yield (Φ_{Total}) of desired products from CO_2 reduction was calculated by using Eqs. (3)–(5) and reported in Table 2:

$$\Phi = \frac{n_e \times M_i}{M_p} \times 100 \quad (3)$$

$$M_p = \frac{I \times S}{N_A \times E} \quad (4)$$

$$\Phi_{Total} = \Phi_{C_2H_4} + \Phi_{C_2H_6} \quad (5)$$

where n_e is number of electrons required to transform CO_2 to products (12 and 14 electrons for C_2H_4 and C_2H_6, respectively), M_i is mole of each product (C_2H_4 and C_2H_6), M_p is mole of photon absorbed by catalyst, I is light intensity (0.37 mW cm^{-2}), S is area exposed to light (170.91 cm^2), N_A is Avogadro's number (6.022×10^{23} mol^{-1}), and E is photon energy (3.61×10^{-19} J at 555 nm). The total quantum yields of desired products obtained from undoped TiO_2 and 0.5Sp/10N–TiO_2 catalysts under visible light irradiation ranged from 0.005 to 0.060%. In comparison, the quantum yields of 0.5Sp/10N–TiO_2 catalyst in this study show better efficiency in CO_2 reduction — approximately 2.54 times and 1.50 times those reported by Nguyen et al. [33] (for CO_2 reduction to C_2H_4 product over 0.5Cu–0.5Fe/TiO_2 catalyst coated optical fibers under an artificial light (320–500 nm)), and Lee et al. [42] (for CO_2 reduction to CH_3CHO and CH_3OCHO products over LHCII/Rh–TiO_2 catalyst), respectively.

3.6. Proposed reaction mechanism for hydrogen and hydrocarbon products syntheses over Spirulina-modified TiO_2 catalysts

Based on the information regarding electron paramagnetic resonance (EPR) spectroscopy and diffuse reflectance infrared Fourier transform spectroscopy (DRIFTS) that has been reported [81–84], CO_2^- and $CH_3^\bullet$ were found to be major intermediates for CH_4 production in a solid–liquid reaction system, while HCO_3^- and $C^\bullet$ were the intermediates for hydrocarbon production in a solid–gas reaction system. Accordingly, the possible reaction pathways of CO_2 reduction for the formation of hydrogen and hydrocarbon products in this present work are deduced as follows, and the reaction mechanism is illustrated in Fig. 11.

$$chl \xrightarrow{h\nu} {}^1chl^* \xrightarrow{ISC} {}^3chl^* \quad (R1)$$

$${}^1chl^*, {}^3chl^* \rightarrow chl^+ + e^- \quad (R2)$$

$$chl^+ + ED \rightarrow chl + ED^+ \quad (R3)$$

$$Ti\,O_2 \xrightarrow{h\nu} e^-_{CB} + h^+_{VB} \quad (R4)$$

$$H_2O + h^+ \rightarrow H^+ + OH^\bullet \quad (R5)$$

$$H^+ + e^- \rightarrow H^\bullet \quad (R6)$$

$$H^\bullet + H^\bullet \rightarrow H_2 \quad (R7)$$

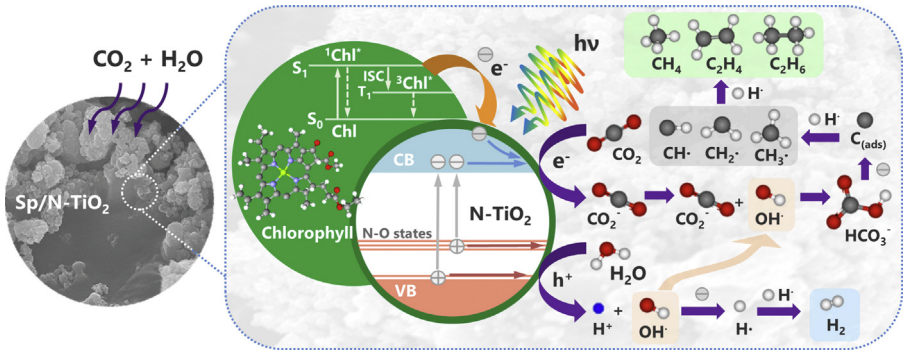

Fig. 11. Proposed mechanism for photoreduction of CO_2 with water on *Spirulina*-modified N–TiO_2 catalyst.

$$CO_2 + e^- \rightarrow CO_2^- \quad \text{(R8)}$$

$$CO_2 + Ti^{3+} \rightarrow Ti^{4+} - CO_2^- \rightarrow Ti^{4+} + CO_2^- \quad \text{(R9)}$$

$$CO_2^- + OH^\bullet \rightarrow HCO_3^- \quad \text{(R10)}$$

$$HCO_3^- + e^- \rightarrow C_{(ads)}{}^\bullet \xrightarrow{H^\bullet} C\,H_3^\bullet \xrightarrow{H^\bullet} CH_4 \quad \text{(R11)}$$

$$C_{(ads)}{}^\bullet \xrightarrow{H^\bullet} CH^\bullet,\ CH_2^\bullet CH_3^\bullet \xrightarrow{H^\bullet} C_2H_4 \quad \text{(R12)}$$

$$CH_3^\bullet + CH_3^\bullet \rightarrow C_2H_6 \quad \text{(R13)}$$

As shown in the schematic in Fig. 11 and (R1), chlorophyll (chl) primarily absorbs light energy, which excites an electron from a ground state to an excited singlet state ($^1chl^*$), and some electrons undergo intersystem crossing (ISC) to theirs triplet state ($^3chl^*$). In the excited state, an electron can readily release and transfer to TiO_2, while chlorophyll ($^1chl^*$, $^3chl^*$) simultaneously converts to its cationic form (chl^+ in (R2)) which can be regenerated back to chlorophyll (chl) by receiving electron from an electron donor (ED) in *Spirulina* or react with some decomposed compounds from *Spirulina* as shown in (R3). At the same time, TiO_2 creates electron–hole pairs on its surface by absorbing sufficient light energy (R4). For H_2 formation, water consecutively reacts with holes on the catalysts and produces H_2 through the formation of H^+ ions and $H^\bullet$ radicals as shown in (R5)–(R7).

The formation pathways of hydrocarbon products shown in (R8)–(R13) are more complicated than those of H_2 since more electrons and protons are incorporated. CO_2 firstly reacts with electron in (R8) or Ti^{3+} in (R9) to form CO_2^-, which can be further reduced to surface HCO_3^- (R10). After that HCO_3^- then reacts with an electron in (R11) to form $C_{(ads)}^\bullet$ radicals, which possibly convert to CH_4, C_2H_4, and C_2H_6 in (R11)–(R13) by reacting with $H^\bullet$ radicals. Due to the complexity of the reaction mechanism for hydrocarbon productions, future study using EPR and DRIFTS will be helpful to confirm this proposed mechanism and reaction intermediates.

4. Conclusion

Spirulina-modified N-doped TiO_2 (Sp/N–TiO_2) catalysts were successfully synthesized and found to significantly influence the catalytic performance for CO_2 photoreduction under visible light. The photocatalytic activities of TiO_2 catalysts were increased by doping nitrogen into TiO_2 lattice and further enhanced by loading *Spirulina* onto the catalysts. Nitrogen dopants in the form of interstitial N that generated impurity energy levels of N—O states above the TiO_2 maximum valence band and the surface V_O as the active adsorption sites of reactants and intermediates were responsible for the increase in visible light activity of the N–TiO_2 catalysts. For Sp/N–TiO_2 catalysts, the chlorophyll in *Spirulina* helps improve the photocatalytic efficiency by acting as a photosensitizer and donates electrons to N–TiO_2 catalysts. Moreover, these additional electrons also improve the stability of photocatalysts and promote the chain growth probability of C_2H_6, resulting in the increase of C_{2+} product selectivity. The highest C_{2+} product selectivity was observed from 0.5Sp/10N–TiO_2 catalyst, for which the selectivity is approximately 7.5 times and 4.6 times higher than those of undoped TiO_2 and 10N–TiO_2 catalysts, respectively. However, it should be noted that the activities of the catalysts were decreased with high percentages of modifiers as their use possibly led to the formation of electron–hole pair recombination.

Acknowledgements

This work was financially supported by grants from the Thailand Research Fund through the Royal Golden Jubilee Ph.D. Program (Grant No. PHD/0074/2554), the Center for Advanced Studies in Nanotechnology for Chemical, Food and Agricultural Industries, Rayong Institute of Science and Technology Foundation, and the Kasetsart University Research and Development Institute (KURDI). The authors would like to thank the support from the Synchrotron Light Research Institute (Public Organization), SLRI, Thailand for XPS and XAS measurements.

Appendix A. Supplementary data

Supplementary data associated with this article can be found, in the online version, at http://dx.doi.org/10.1016/j.apcatb.2014.12.022.

References

[1] N.S. Lewis, D.G. Nocera, Proc. Natl. Acad. Sci. U.S.A. 103 (2006) 15729–15735.
[2] T.R. Cook, D.K. Dogutan, S.Y. Reece, Y. Surendranath, T.S. Teets, D.G. Nocera, Chem. Rev. 110 (2010) 6474–6502.
[3] C. Song, Catal. Today 115 (2006) 2–32.
[4] S. Solomona, G.-K. Plattnerb, R. Knuttic, P. Friedlingstein, Proc. Natl. Acad. Sci. U.S.A. 106 (2009) 1704–1709.
[5] D. Lüthi, M.L. Floch, B. Bereiter, T. Blunier, J.-M. Barnola, U. Siegenthaler, D. Raynaud, J. Jouzel, H. Fischer, K. Kawamura, T.F. Stocker, Nature 453 (2008) 379–382.
[6] S. Kiatphuengporn, M. Chareonpanich, J. Limtrakul, Chem. Eng. J. 240 (2014) 527–533.
[7] W. Donphaia, K. Faungnawakij, M. Chareonpanich, J. Limtrakul, Appl. Catal. A 475 (2014) 16–26.
[8] J. Tollefson, Nature 473 (2011) 134–135.
[9] J. Barber, Chem. Soc. Rev. 38 (2009) 185–196.
[10] R. Ceulemans, I.A. Janssens, M.E. Jach, Am. Bot. 84 (1999) 577–590.
[11] R.M. Gifford, Funct. Plant Biol. 30 (2003) 171–186.
[12] S. Murata, H. Furukawa, K. Kuroda, Chem. Mater. 13 (2001) 2722–2729.
[13] P. Usubharatana, D. McMartin, A. Veawab, P. Tontiwachwuthikul, Ind. Eng. Chem. Res. 45 (2006) 2558–2568.
[14] S.C. Roy, O.K. Varghese, M. Paulose, C.A. Grimes, ACS Nano 4 (2010) 1259–1278.
[15] M. Kitano, M. Matsuoka, M. Ueshima, M. Anpo, Appl. Catal. A 325 (2007) 1–14.
[16] G.K. Mor, O.K. Varghese, M. Paulose, K. Shankar, C.A. Grimes, Sol. Energy Mater. Sol. Cells 90 (2006) 2011–2075.

[17] R. Asahi, T. Morikawa, T. Ohwaki, K. Aoki, Y. Taga, Science 293 (2001) 269–271.
[18] K. Li, T. Chen, L. Yan, Y. Dai, Z. Huang, H. Guo, L. Jiang, X. Gao, J. Xiong, D. Song, Catal. Commun. 28 (2012) 196–201.
[19] O.K. Varghese, M. Paulose, T.J. LaTempa, C.A. Grimes, Nano Lett. 9 (2009) 731–737.
[20] S. In, A. Orlov, R. Berg, F. García, S. Pedrosa-Jimenez, M.S. Tikhov, D.S. Wright, R.M. Lambert, J. Am. Chem. Soc. 129 (2007) 13790–13791.
[21] J.C. Yu, J. Yu, W. Ho, Z. Jiang, L. Zhang, Chem. Mater. 14 (2002) 3808–3816.
[22] S.U.M. Khan, M. Al-Shahry, W.B. Ingler Jr., Science 297 (2002) 2243–2245.
[23] W. Su, Y. Zhang, Z. Li, L. Wu, X. Wang, J. Li, X. Fu, Langmuir 24 (2008) 3422–3428.
[24] S. Rehman, R. Ullah, A.M. Butt, N.D. Gohar, J. Hazard. Mater. 170 (2009) 560–569.
[25] R. Asahi, T. Morikawa, Chem. Phys. 339 (2007) 57–63.
[26] C.D. Valentin, G. Pacchioni, A. Selloni, S. Livraghi, E. Giamello, J. Phys. Chem. Lett. 109 (2005) 11414–11419.
[27] C.D. Valentin, E. Finazzi, G. Pacchioni, A. Selloni, S. Livraghi, M.C. Paganini, E. Giamello, Chem. Phys. 339 (2007) 44–56.
[28] N. Sasirekha, S.J.S. Basha, K. Shanthi, Appl. Catal. B 62 (2006) 169–180.
[29] C. Zhao, A. Krall, H. Zhao, Q. Zhang, Y. Li, Int. J. Hydrogen Energy 37 (2012) 9967–9976.
[30] M. Hamadanian, A. Reisi-Vanani, A. Majedi, Appl. Surf. Sci. 256 (2010) 1837–1844.
[31] I. Tseng, J.C.-S. Wu, Catal. Today 97 (2004) 113–119.
[32] Y. Li, W. Wang, X. Qiu, L. Song, H.M. Meyer III, M.P. Paranthaman, G. Eres, Z. Zhang, B. Gu, Appl. Catal. B 110 (2011) 148–153.
[33] T.-V. Nguyen, J.C.S. Wu, C.-H. Chiou, Catal. Commun. 9 (2008) 2073–2076.
[34] O. Ozcan, F. Yukruk, E.U. Akkaya, D. Uner, Appl. Catal. B 71 (2007) 291–297.
[35] X.-H. Xia, Z.-J. Jia, Y. Yu, Y. Liang, Z. Wang, L.-L. Ma, Carbon 45 (2007) 717–721.
[36] V. Štengl, D. Popelková, P. Vláčil, J. Phys. Chem. C 115 (2011) 25209–25218.
[37] T.W. Woolerton, S. Sheard, E. Reisner, E. Pierce, S.W. Ragsdale, F.A. Armstrong, J. Am. Chem. Soc. 132 (2010) 2132–2133.
[38] H. Hagiwara, T. Inoue, K. Kaneko, T. Ishihara, Chem. Eur. J. 15 (2009) 12862–12870.
[39] Y.-S. Lai, Y.H. Su, M.I. Lin, Dyes Pigm. 103 (2014) 76–81.
[40] M. Joshi, S.P. Kamble, N.K. Labhsetwar, D.V. Parwate, S.S. Rayalu, J. Photochem. Photobiol. A 204 (2009) 83–89.
[41] S. Benjamin, D. Vaya, P.B. Punjabi, S.C. Ameta, Arabian J. Chem. 4 (2011) 205–209.
[42] C.-W. Lee, R.A. Kourounioti, J.C.S. Wu, E. Murchie, M. Maroto-Valer, O.E. Jensen, C.-W. Huang, A. Ruban, J. CO_2 Util. 5 (2014) 33–40.
[43] E.D.G. Danesi, C.O. Rangel-Yagui, J.C.M. Carvalho, S. Sato, Biomass Bioenergy 26 (2004) 329–335.
[44] R. Henrikson, Earth food Spirulina, Ronore Enterprises Inc., California, 1989.
[45] C. de, O. Rangel-Yagui, E.D.G. Danesi, J.C.M. de Carvalho, S. Sato, Bioresour. Technol. 92 (2004) 133–141.
[46] G.C. Collazzo, E.L. Foletto, S.L. Jahn, M.A. Villetti, J. Environ. Manage. 98 (2012) 107–111.
[47] D. Bajracharya, Experiments in Plant Physiology, Narosa Publishing House, New Delhi, 1999.
[48] K. Kočí, L. Obalová, L. Matějová, D. Plachá, Z. Lacný, J. Jirkovský, O. Šolcová, Appl. Catal. B 89 (2009) 494–502.
[49] I. Tseng, W.-C. Chang, J.C.S. Wu, Appl. Catal. B 37 (2002) 37–48.
[50] C. Song, X. Zhang, C. Jia, P. Zhou, X. Quan, C. Duan, Talanta 81 (2010) 643–649.
[51] S.-H. Liu, H.-R. Syu, Appl. Energy 100 (2012) 148–154.
[52] Y.Y. Gurkan, N. Turkten, A. Hatipoglu, Z. Cinar, Chem. Eng. J. 184 (2012) 113–124.
[53] D.-R. Liu, C.-D. Wei, B. Xue, X.-G. Zhang, Y.-S. Jiang, J. Hazard. Mater. 182 (2010) 50–54.
[54] W.-Q. Wu, H.-S. Rao, Y.-F. Xu, Y.-F. Wang, C.-Y. Su, D.-B. Kuang, Sci. Rep. 3 (2013) (ID 1892).
[55] J. Liao, L. Shi, S. Yuan, Y. Zhao, J. Fang, J. Phys. Chem. C 113 (2009) 18778–18783.
[56] R. Beranek, H. Kisch, Photochem. Photobiol. Sci. 7 (2008) 40–48.
[57] F. Xu, Q.-A. Zhou, J.-X. Sun, C.-F. Liu, J.-L. Ren, R.-C. Sun, S. Curling, P. Fowler, M.S. Baird, Process Biochem. 42 (2007) 913–918.
[58] Z. Mehraban, F. Farzaneh, A. Shafiekhani, Opt. Mater. 29 (2007) 927–931.
[59] G.-S. Shao, X.-J. Zhang, Z.-Y. Yuan, Appl. Catal. B 82 (2008) 208–218.
[60] X. Li, Z. Zhuang, W. Li, H. Pan, Appl. Catal. A 429–430 (2012) 31–38.
[61] S. Sato, R. Nakamura, S. Abe, Appl. Catal. A 284 (2005) 131–137.
[62] X. Chen, P.-A. Glans, X. Qiu, S. Dayal, W.D. Jennings, K.E. Smith, C. Burda, J. Guo, J. Electron. Spectrosc. Relat. Phenom. 162 (2008) 67–73.
[63] M. Trytek, E. Janik, W. Maksymiec, J. Fiedurek, A. Lipke, M. Majdan, J. Photochem. Photobiol. A 223 (2011) 14–24.
[64] L. Lin, R.Y. Zheng, J.L. Xie, Y.X. Zhu, Y.C. Xie, Appl. Catal. B 76 (2007) 196–202.
[65] G.-S. Shao, F.-Y. Wang, T.-Z. Ren, Y. Liu, Z.-Y. Yuan, Appl. Catal. B 92 (2009) 61–67.
[66] J. Yuan, M. Chen, J. Shi, W. Shangguan, Int. J. Hydrogen Energy 31 (2006) 1326–1331.
[67] U. Diebold, Surf. Sci. Rep. 48 (2003) 53–229.
[68] M. Ceotto, L.L. Presti, G. Cappelletti, D. Meroni, F. Spadavecchia, R. Zecca, M. Leoni, P. Scardi, C.L. Bianchi, S. Ardizzone, J. Phys. Chem. C 116 (2012) 1764–1771.
[69] F. Peng, L. Cai, H. Yu, H. Wang, J. Yang, J. Solid State Chem. 181 (2008) 130–136.
[70] D.P. Acharya, N. Camillone, P. Sutter, J. Phys. Chem. C 115 (2011) 12095–12105.
[71] H. He, P. Zapol, L.A. Curtiss, J. Phys. Chem. C 114 (2010) 21474–21481.
[72] W.-N. Wang, W.-J. An, B. Ramalingam, S. Mukherjee, D.M. Niedzwiedzki, S. Gangopadhyay, P. Biswas, J. Am. Chem. Soc. 134 (2012) 11276–11281.
[73] Y. Li, W.-N. Wang, Z. Zhan, M.-H. Woo, C.-Y. Wu, P. Biswas, Appl. Catal. B 100 (2010) 386–392.
[74] I. Tseng, J.C.S. Wu, H.-Y. Chou, J. Catal. 221 (2004) 432–440.
[75] D. Pei , J. Luan, 2012, Int. J. Photoenergy 2012. (ID 262831).
[76] A. Kathiravan, M. Chandramohan, R. Renganathan, S. Sekar, Spectrochim. Acta Part A 71 (2009) 1783–1787.
[77] L. Yuliati, H. Itoh, H. Yoshida, Chem. Phys. Lett. 452 (2008) 178–182.
[78] T.-V. Nguyen, J.C.S. Wu, Appl. Catal. A 335 (2008) 112–120.
[79] M.R. Dubois, D.L. Dubois, Acc. Chem. Res. 42 (2009) 1974–1982.
[80] C.-C. Yang, J. Vernimmen, V. Meynen, P. Cool, G. Mul, J. Catal. 284 (2011) 1–8.
[81] M. Anpo, H. Yamashita, Y. Ichihashi, S. Ehara, J. Electroanal. Chem. 396 (1995) 21–26.
[82] N.M. Dimitrijevic, B.K. Vijayan, O.G. Poluektov, T. Rajh, K.A. Gray, H. He, P. Zapol, J. Am. Chem. Soc. 133 (2011) 3964–3971.
[83] L. Liu, H. Zhao, J.M. Andino, Y. Li, ACS Catal. 2 (2012) 1817–1828.
[84] L. Liu, Y. Li, Aerosol Air Qual. Res. 14 (2014) 453–469.